Article

Cell Host & Microbe

In Vitro Culture, Drug Sensitivity, and Transcriptome of *Plasmodium Vivax* Hypnozoites

Graphical Abstract

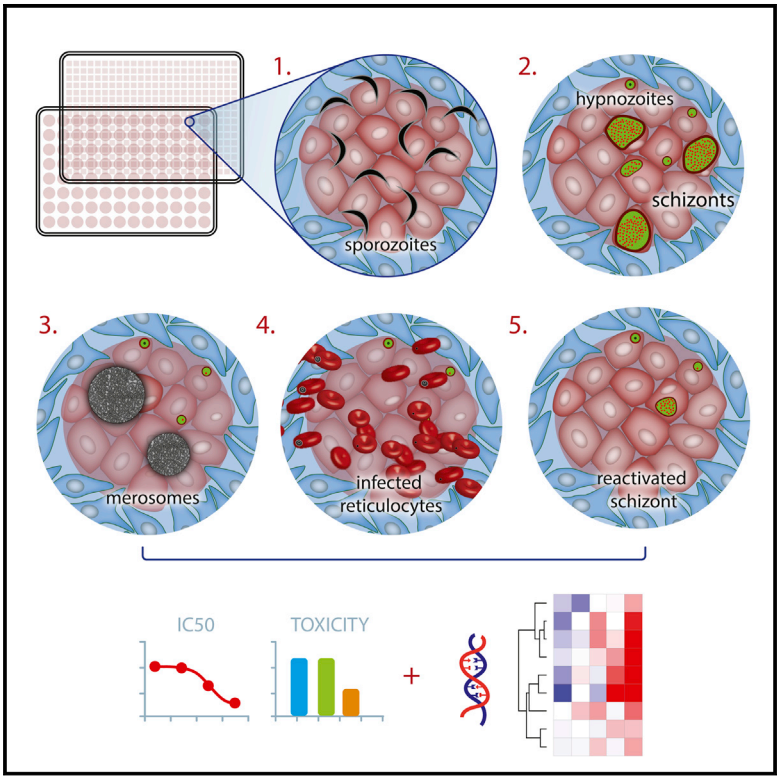

Highlights

- The MPCC platform supports formation and reactivation of hypnozoites *in vitro*
- *P. vivax* schizonts in the MPCCs mature, release merosomes, and infect reticulocytes
- Hybrid capture and RNA sequencing reveals the hypnozoite transcriptome in the MPCCs
- MPCCs allow prophylactic and radical cure testing of anti-hypnozoite drugs

Authors

Nil Gural, Liliana Mancio-Silva, Alex B. Miller, ..., Sandra March, Jetsumon Sattabongkot, Sangeeta N. Bhatia

Correspondence

sbhatia@mit.edu

In Brief

Plasmodium vivax hypnozoites are difficult to study due to the lack of human liver platforms. Gural et al. recapitulated the entire liver stage of *P. vivax in vitro*, including formation and reactivation of hypnozoites and release of merosomes. Hybrid capture followed by RNA-seq revealed a first look into the hypnozoite transcriptome.

Gural et al., 2018, Cell Host & Microbe *23*, 1–12
March 14, 2018
https://doi.org/10.1016/j.chom.2018.01.002

CellPress

Please cite this article in press as: Gural et al., *In Vitro* Culture, Drug Sensitivity, and Transcriptome of *Plasmodium Vivax* Hypnozoites, Cell Host & Microbe (2018), https://doi.org/10.1016/j.chom.2018.01.002

Cell Host & Microbe
Article

In Vitro Culture, Drug Sensitivity, and Transcriptome of *Plasmodium Vivax* Hypnozoites

Nil Gural,[1,7,8] Liliana Mancio-Silva,[1,8] Alex B. Miller,[2,8] Ani Galstian,[2] Vincent L. Butty,[3] Stuart S. Levine,[3] Rapatbhorn Patrapuvich,[4] Salil P. Desai,[5] Sebastian A. Mikolajczak,[6] Stefan H.I. Kappe,[6] Heather E. Fleming,[1,8] Sandra March,[1,2,8] Jetsumon Sattabongkot,[4] and Sangeeta N. Bhatia[1,2,7,8,9,10,*]

[1]Harvard-MIT Department of Health Sciences and Technology, Institute for Medical Engineering and Science, Massachusetts Institute of Technology, Boston, MA 02142, USA
[2]Broad Institute, Boston, MA 02142, USA
[3]BioMicro Center, Massachusetts Institute of Technology, Boston, MA 02142, USA
[4]Mahidol Vivax Research Unit, Faculty of Tropical Medicine Mahidol University, Bangkok 10400, Thailand
[5]Phenomyx LLC, Boston, MA 02139, USA
[6]Center for Infectious Disease Research, Seattle, WA 98109, USA
[7]Howard Hughes Medical Institute, Chevy Chase, MD 20815, USA
[8]Koch Institute for Integrative Cancer Research, Boston, MA 02142, USA
[9]Department of Medicine, Brigham and Women's Hospital Boston, Boston, MA 02115, USA
[10]Lead Contact
*Correspondence: sbhatia@mit.edu
https://doi.org/10.1016/j.chom.2018.01.002

SUMMARY

The unique relapsing nature of *Plasmodium vivax* infection is a major barrier to malaria eradication. Upon infection, dormant liver-stage forms, hypnozoites, linger for weeks to months and then relapse to cause recurrent blood-stage infection. Very little is known about hypnozoite biology; definitive biomarkers are lacking and *in vitro* platforms that support phenotypic studies are needed. Here, we recapitulate the entire liver stage of *P. vivax in vitro*, using a multiwell format that incorporates micropatterned primary human hepatocyte co-cultures (MPCCs). MPCCs feature key aspects of *P. vivax* biology, including establishment of persistent small forms and growing schizonts, merosome release, and subsequent infection of reticulocytes. We find that the small forms exhibit previously described hallmarks of hypnozoites, and we pilot MPCCs as a tool for testing candidate anti-hypnozoite drugs. Finally, we employ a hybrid capture strategy and RNA sequencing to describe the hypnozoite transcriptome and gain insight into its biology.

INTRODUCTION

Since it was first reported in 2700 BC, the malaria parasite *Plasmodium* has successfully evaded all attempts at eradication. Combined, the two most prevalent human *Plasmodium* species put 3.2 billion people at risk of malaria infection (WHO, 2015). *Plasmodium* parasites enter the blood stream via the bite of an infected *Anopheles* mosquito, travel to the liver, and invade hepatocytes. In this obligate, yet clinically silent stage, the invading sporozoites develop and replicate by schizogony, forming thousands of new haploid parasites called merozoites. Upon completion of the liver stage, merozoites are released into the blood to infect erythrocytes, initiating the cyclic and symptomatic blood stage. While *Plasmodium falciparum* is responsible for the majority of malaria-associated deaths, *P. vivax* presents a bigger barrier to eradication due to its propensity to cause chronic, relapsing disease weeks to years after the original infection. This species-specific aspect of *P. vivax* biology was discovered, only three decades ago, to be caused by a dormant liver-stage form of the parasite, termed the hypnozoite. Originally identified in livers of rhesus monkeys infected with *Plasmodium cynomolgi* (Krotoski et al., 1980), the hypnozoite remains a relative biological mystery. In the absence of specific molecular or phenotypic markers, hypnozoites are generally described as small, uninucleate forms that persist for weeks to months after the initial infection (Krotoski et al., 1982), do not express late liver-stage antigens, are sensitive to the only clinically available hypnozoite-targeting drug (Dembele et al., 2011), and have the potential to relapse. Functionally, the cues that cause dormancy or promote reactivation are still poorly understood. This limited knowledge surrounding hypnozoite biology, due in large part to limited access to *P. vivax* sporozoites and the inability to establish primary human hepatocyte (PHH) cultures, has stymied drug development and represents a barrier to eradication. Today, the only clinically available hypnozoite-eliminating drug, primaquine, has an unknown mechanism of action and is contraindicated in a subset of the population in which a glucose-6-dehydrogenase enzyme deficiency causes hemolysis upon administration of the drug (Wells et al., 2010). Moreover, increasing prevalence of drug resistance against blood stages (Price et al., 2014) underscores the urgent need for new liver-stage-targeting agents, yet in order to develop new interventions, robust *in vitro* models that facilitate hypnozoite characterization, allow assessment of drug sensitivity, and help uncover cues that prompt both dormancy and reactivation are needed.

Historically, examples of successful *in vitro* culture of liver-stage *P. vivax* are extremely limited. While *P. vivax* schizonts

were first visualized in PHHs (Mazier et al., 1984), small forms were only reported in hepatoma cell lines, HepG2-A16 and HC04, after 9–14 days of culture (Chattopadhyay et al., 2010; Hollingdale et al., 1985; Sattabongkot et al., 2006). Yet, the ongoing proliferation of infected hepatoma cells limited the utility of these platforms for the long-term assays necessary to interrogate *P. vivax* hypnozoite development. We have developed a microscale human liver platform that combines PHHs with supportive stromal cells in a multiwell micropatterned co-culture format (Khetani and Bhatia, 2008), where stable hepatocyte-specific function and metabolism is observed for 4–6 weeks. This platform supports infection with hepatitis C and B viruses, *P. falciparum* and *P. vivax* (reviewed in Gural et al., 2018; March et al., 2015). In addition to providing a permissive host, hepatocytes cultured in micropatterned primary human hepatocyte co-cultures (MPCCs) exhibit human-specific drug metabolism and long-term stability, ideal traits for drug screening and studies of long-term dormancy and reactivation.

In this study, we progressed beyond our previous preliminary findings and confirmed the hypnozoite identity of small forms present in the MPCC system using clinical Thai *P. vivax* isolates. Specifically, we found that small forms exhibit the known hallmarks of hypnozoites in that they are small, uninucleate, persistent for weeks, negative for late-stage liver antigens, sensitive to primaquine, and appear to have the capacity to reactivate. Furthermore, our multiwell *in vitro* platform enabled transcriptional characterization of both small and large *P. vivax* liver-stage forms, by using a customized capture method prior to RNA sequencing (RNA-seq). To demonstrate its potential as a drug screening platform, we compared the effectiveness of six clinical candidates in multipoint dosing. Finally, we have re-engineered the MPCCs to support a 384-well format, paving the way for fully automated high-throughput drug screening. Collectively, the data presented here highlight the potential of MPCCs to enhance our understanding of hypnozoite biology and advance drug development against this stage of the *P. vivax* life cycle.

RESULTS

Infection with Clinical *P. vivax* Isolates Yields Hypnozoites and Schizonts in MPCCs

Previous work with *P. vivax* in the MPCCs has been performed with cryopreserved sporozoites passaged through monkeys. To establish liver-stage hallmarks of clinical Thai *P. vivax* isolates, we infected MPCCs with sporozoites obtained from freshly dissected *Anopheles dirus* mosquitoes (Figure 1A). To assess growth kinetics, we fixed cultures over a series of time points, using two *P. vivax* subtypes observed in Thailand, VK210 and VK247, which differ in their central repeated region of the circumsporozoite protein (CSP) (Rosenberg et al., 1989). Both subtypes successfully infected PHHs, and gave rise to a subpopulation of exo-erythrocytic forms (EEFs) that grew in size, and a subpopulation of EEFs that remained small (Figure 1B). While day 5 forms were small, a bimodal separation of small and large forms became pronounced on day 8 for both subtypes tested. Consistent with clinical human data that reported *P. vivax* schizonts of up to 42 μm in diameter in a human liver biopsy (Shortt and Garnham, 1948), EEFs in day 8 MPCCs ranged from 7 to 80 μm in diameter. We further quantified day 10 forms and observed parasites as large as 130 μm in diameter (data not shown). To determine parasite development and maturation *in vitro*, we tested reactivity to an antibody against the merozoite surface protein 1 (MSP1) (Combe et al., 2009). At the earliest time point tested, 5 days post-infection, no MSP1 expression was observed (Figure 1C), while on day 8 post-infection, large parasites but not small forms were positive for MSP1. Remarkably, day 18 and 21 cultures of *P. vivax* sporozoites of both strains exhibited persistent small forms (Figures 1B and S1B), which, based on their size, morphology, lack of MSP1 expression, and lack of growth, were considered candidate hypnozoites.

Upon completion of its liver-stage development, *Plasmodium* parasites emerge from the host hepatocytes within membrane-bound vesicles; known as merosomes (Sturm et al., 2006). These structures contain the erythrocyte-invading merozoites. A hallmark of EEF maturation, merosome release, was observed in live cultures on days 11 and 12 (Figures 1D and S1A; Movies S1, S2, and S3). Furthermore, to confirm that MPCCs support the full liver-stage life cycle of human malaria, MPCCs were overlaid with packed red blood cells, of which 33% were reticulocytes. Up to 1% of red blood cells (3% of reticulocytes) overlaid 10 days post-infection became positive for ring-stage *P. vivax* parasites, as assessed by analysis of Giemsa-stained smears on day 11 (Figure 1E). In two additional independent experiments, smears of overlaid reticulocytes were negative on day 8 post-infection but became positive on day 9.

To assay for longitudinal changes in cellular organelles in parasites, we used several antibodies targeted against *P. vivax*. Developing EEFs were visualized using an antibody that recognizes the parasitophorous vacuole membrane (PVM) (Mikolajczak et al., 2015). Over time, the PVM expanded, encapsulating the growing number of merozoites and isolating the parasite cytoplasm from that of the host (Figure 1F). Recently, in a humanized mouse model of *P. vivax* infection, a coalescence of UIS4, termed the "prominence," has been proposed as a candidate hypnozoite marker, based on its exclusive observation in small forms found in sections of infected chimeric mouse livers (Mikolajczak et al., 2015). In contrast, in MPCC cultures, a UIS4 prominence is observed both in small forms and in a subpopulation of large forms (Figure S1C). The endoplasmic reticulum of the parasite was visualized using an anti-binding immunoglobulin protein antibody (Noe et al., 2000) (Figure 1F). The structure appeared as a network that expanded in size and complexity as the parasite developed, and that included punctate bright spots of varying sizes. The mitochondria, visualized via the heat-shock protein 60 (HSP60), formed a vast, scaffold-like network surrounding the individual nuclei of the EEFs on day 8 (Figure 1F). During the 3-day growth period depicted, detection of the individual nuclei became difficult using the DAPI stain, especially in candidate hypnozoites, so we employed an additional nuclear antibody to track histone-acetylation marks (H3K9Ac), previously shown to stain *P. vivax* nuclei (Mikolajczak et al., 2015). While small forms maintained a single nuclear structure, growing schizonts contained numerous nuclei (Figure 1F). Day 8 forms were further visualized using antibodies against heat-shock protein 70 (HSP70) and macrophage inhibitory factor (Miller et al., 2012). The cytoplasm of the parasites expanded in growing schizonts compared to the small forms present at the same time point (Figure 1F). The apicoplast was

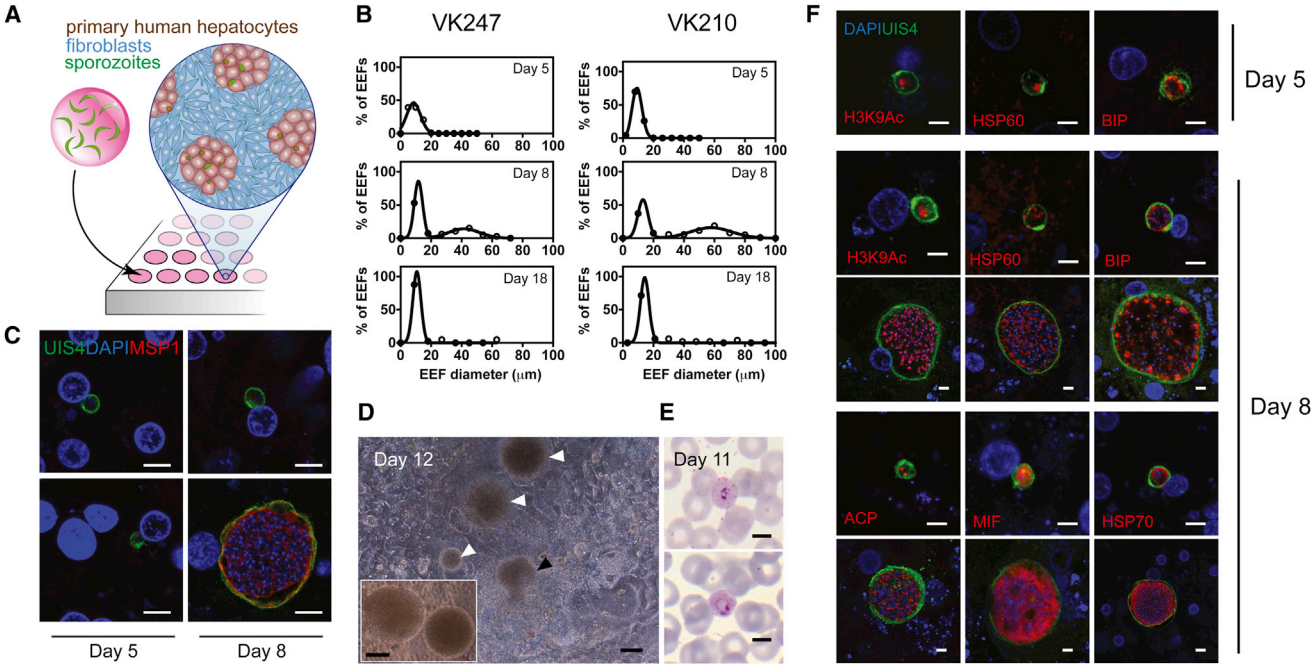

Figure 1. MPCCs Can Be Infected with Clinical *P. vivax* Isolates

(A) Schematic of the MPCC system where primary human hepatocyte (PHH) islands are patterned in 96-well plates. Sporozoites are overlaid onto cultures 1 day post-seeding and incubated for 3 hr, followed by addition of mouse fibroblasts.

(B) Size distribution histograms of *P. vivax* EEFs in the MPCC system are shown after infection with two clinical isolates, performed in two separate experiments. VK247 experiment: day 5, 310 parasites; day 8, 199 parasites; day 18, 49 parasites. VK210 experiment: day 5, 207 parasites; day 8, 179 parasites; day 18, 41 parasites. At least three wells per time point pooled. See also Figure S1B.

(C) Representative images of small and large parasites on days 5 and 8, stained with an anti-MSP1 antibody. Scale bars, 5 μm.

(D) Representative images of merozoite release in live *P. vivax* (VK210) cultures on day 12 (observed in 5 out of 5 wells). Released merosomes (white arrows) and merozoite-releasing merosome are shown (black arrow). Inset shows close-up view of two merosomes on the same day. Scale bars, 50 μm. See also Figure S1A and Movies S1, S2, and S3.

(E) Representative images of *P. vivax* infected reticulocytes. Reticulocyte-enriched red blood cells were overlaid onto *P. vivax*-infected MPCCs, 10 days post-infection. Giemsa staining of collected blood cells revealed ring-stage parasites, 1 day later. Experiment performed three times by adding blood cells to at least six infected wells, all of which became positive for blood-stage infection as assessed by blood smear (6/1,018, 10/1,070, and 4/995 infected red blood cells counted). Scale bars, 5 μm.

(F) *P. vivax* EEFs from MPCC cultures were fixed on days 5 and 8. Antibodies against UIS4, anti-binding immunoglobulin protein (BIP), HSP60, and H3K9Ac were used to visualize parasite structures. Day 8 structures were further characterized with antibodies against HSP70, macrophage inhibitory factor (MIF), and anti-acyl carrier protein (ACP). A representative small and large form is shown for all day 8 proteins. Scale bars, 5 μm. See also Figures S1C and S2.

visualized with an anti-acyl carrier protein antibody and showed a complex, branched expression pattern in growing schizonts versus punctate spots in the small forms (Figure S2). Overall, cellular structures of the *P. vivax* EEFs became more complex over time.

Functional Characterization of Small Forms Fit Pre-existing Hypnozoite Criteria

In addition to the size and kinetic characterization evidence that the small, persistent candidate hypnozoites identified in MPCCs are indeed *bona fide* dormant forms, we performed further functional characterization of the small forms. We treated *P. vivax*-infected MPCCs with two drugs that have been proposed to have differential hypnozoite-killing activity in clinical settings. We characterized the half-maximal inhibitory concentration (IC_{50}) of primaquine and atovaquone on all forms, by assessing the number of parasites remaining in culture when exposed to a range of drug concentrations. Primaquine exhibited an IC_{50} of 0.32 μM (95% confidence interval; 0.26 to 0.4). In contrast, treatment with atovaquone, a drug that is clinically ineffective against hypnozoites, reduced the number of EEFs in culture, but not sufficiently to achieve an IC_{50}, even at the highest concentrations tested (Figure 2A). Indeed, atovaquone eliminated the subpopulation of parasites that were larger than 10 μm in diameter, and left a residual subpopulation of only small forms. Primaquine, on the other hand, had killing activity against both small and large forms, consistent with its clinical use as the only available drug with activity against hypnozoites (Figure 2B).

Day 21 MPCC cultures revealed not only persistent hypnozoites, but also a collection of large schizonts (Figure 2C). The observation of large forms that appear beyond the first wave of merosome release is consistent with the interpretation that they originate from reactivated hypnozoites. These forms exhibited similar size ranges and morphologies as day 8 schizonts, based on their staining pattern with antibodies against MSP1, HSP60, and H3K9Ac (Figure 2D). To support the hypothesis that the large forms detected on day 21 represent reactivated small forms, we treated cultures prophylactically with

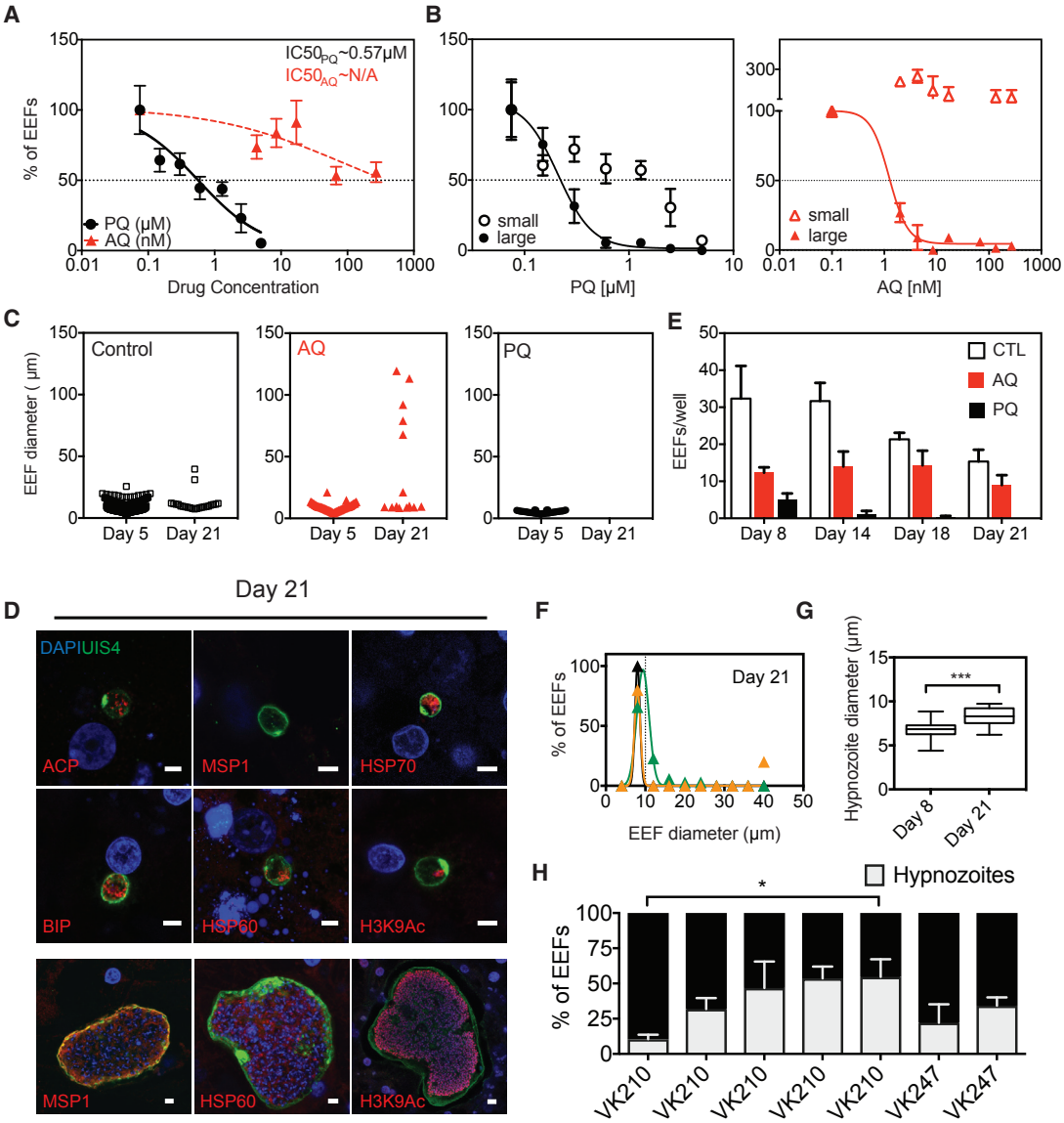

Figure 2. Characterization of Drug Sensitivity, Size, Frequency, and Reactivation of Small Forms in MPCCs Match Hypnozoite Criteria

(A) Primaquine (PQ) and atovaquone (AQ) were dosed at varying concentrations, starting 3 hr post-infection (hpi) and replaced with daily media changes until day 5 when cultures were fixed (prophylactic mode). IC_{50} curves were produced by plotting fraction of EEFs remaining in culture at each concentration, as measured against untreated control wells (mean ± SEM from triplicate wells, representative experiment shown, isolate VK210).

(B) Data from (A) were replotted, after segmenting the populations of parasites into "large" and "small" subpopulations, according to a 10 μm diameter size threshold. Resulting curve fits show differential effect of PQ and AQ on small (<10 μm in diameter) and large (>10 μm in diameter) parasite populations.

(C) Cultures were dosed with PQ (5 μM) or AQ (270 nM) at 3 hpi until day 5. Cultures were maintained with daily media changes until day 21, when the sizes of any remaining parasites were assessed (n = 3 wells per independent experiment. Three experiments pooled for control, two experiments pooled for AQ, one experiment for PQ). See also Figures S3A and S4D.

(D) Representative hypnozoites and candidate reactivated schizonts in day 21 cultures, stained with a panel of antibodies, as indicated. Scale bars, 5 μm. See also Figure S3C.

(E) Number of parasites remaining per well after treatment with PQ or AQ under the same treatment regimen as in (C) (mean ± SEM, n = 3). See also Figure S4D.

(F) Size histograms of day 21 parasites to set a threshold for hypnozoite size (three independent experiments, triplicate wells per experiment).

(G) Hypnozoite diameters from day 8 and day 21 cultures (three independent experiments, triplicate wells per experiment). ***p = 0.0004, two-tailed unpaired t test with Welch's correction.

(H) Hypnozoite frequency was evaluated in six separate experiments on day 8. CSP subtype of each experiment is indicated on the x axis (mean ± SEM shown from at least triplicate wells per experiment. Number of parasites interrogated in each experiment is as follows: 118, 211, 145, 265, 179, 66, 199) *Kruskall-Wallis test.

atovaquone for 5 days in an attempt to deplete large forms. These pre-treated cultures also contained large forms on day 21, consistent with possible reactivation events, where large forms derive from previously dormant hypnozoites (Figure 2C). In an alternative approach, we treated cultures with a different schizonticide from days 5 to 8. While 6 days beyond the last drug treatment, on day 14, cultures solely exhibited small forms, on day 18, one of the cultures revealed re-emergence of large forms (Figure S3A). In contrast, prophylactic primaquine treatment of cultures completely cleared all parasites by day 21 (Figures 2C and 2E). Thus, in the MPCC system, persistent small forms that lack MSP1 expression also display characteristic functional traits of dormant forms: they are differentially drug sensitive to primaquine versus atovaquone, and appear to have the capacity to reactivate. We believe this set of phenotypic attributes supports their classification as *bona fide* hypnozoites.

In the course of our efforts to track the dynamic phenotype of *P. vivax* EEFs in MPCCs, our kinetic analysis has revealed that in addition to their capacity for reactivation, and despite their dormant appearance, hypnozoite sizes increase slightly over time (7–10 μm; Figures 2G and S3B), consistent with a previous description (Mikolajczak et al., 2015). Finally, the relative incidence of hypnozoite forms that arise after infection with a given *P. vivax* sporozoite pool was quantified. In our cultures, hypnozoite frequencies measured on day 8 ranged from 11% to 48%, and were independent of the CSP subtype of the parasite (Figure 2H).

Hypnozoites Cultured in the MPCCs Provide an Antimalarial Testing Platform

An important clinical reality faced by providers is that primaquine sensitivity of patients is variable, in part due to differences in CYP2D6 metabolism, the enzyme complex thought to be primarily responsible for primaquine bioactivation. Thus, not all patients respond similarly to primaquine (Bennett et al., 2013). The MPCC system has the potential to more closely predict not only clinical outcomes related to treatment with drugs such as primaquine that require adequate metabolic activity, but also liver toxicity in donor contexts, which is a major problem in clinical drug development (Kaplowitz, 2005).

To query whether the MPCC platform can detect patient-specific variations in drug responsiveness, we interrogated the primaquine IC_{50} values obtained using different donors. MPCCs established with PHHs isolated from two different human donors were infected with the same *P. vivax* clinical isolate and showed a 6-fold difference in their responsiveness to primaquine (Figure 3A). This result is consistent with a 2-fold change in CYP2D6 activity between the two PHHs, in that the more sensitive cells exhibit 2-fold higher CYP2D6 activity (Figure S4A). Thus, infection of MPCCs can model complex patient-specific phenotypes that arise from a combination of host biology and drug metabolism. Notably, only relatively common genotypes are available using PHHs. For rare genotypes, induced pluripotent stem cells provide a complementary platform to study drug efficacy in a defined host (Berger et al., 2015; Ng et al., 2015).

Having established that MPCC infections can replicate clinical drug responsiveness outcomes using existing antimalarials, we applied our platform to assess the potential effectiveness of novel candidate compounds: four compounds (LMV599, KDU691, MMV390048, and MMV674594) that target the lipid kinase phosphatidylinositol-4-OH kinase (PI4K) (Ghidelli-Disse et al., 2014; McNamara et al., 2013; Younis et al., 2012), one compound (DDD107498) that targets translation elongation factor 2 (eEF2) in *P. falciparum* with activity against *P. vivax* blood stages (Baragaña et al., 2015), and one compound (KAF156) with an unknown mechanism of action (Kuhen et al., 2014) (Figures 3A–3D, S4B, and S4C). All drugs were tested under two dosing regimens, termed "prophylactic" (dosing day 0 to 5) and "radical cure" (dosing day 5 to 8), and the effect of each drug on both parasite number and size were recorded on day 8 (Figure 3A). In prophylactic mode, the four PI4K inhibitors tested had varying activity on both small and large forms (Figure 3D). LMV599, the most potent of the four, cleared all parasites even at the lowest concentration tested. The other three PI4K inhibitors tested had similar IC_{50} values and achieved complete clearance. Notably, the PI4K inhibitors tested were more potent than primaquine, which was most effective at 5 μM. DDD107498 and the most potent PI4K inhibitor tested had similar IC_{50}s, and KAF156, although less potent, had activity against both small and large forms. In radical cure mode, the compounds tested appeared less efficacious. PI4K inhibitors had activity against large forms but not all small forms were cleared from culture. KDU691 cleared a majority of large forms in radical cure mode, in contrast with the relatively small impact of KAF156 using this dosing regimen (Figure 3C). In fact, neither DDD107498 nor KAF156 caused as significant a reduction in parasite number as the PI4K inhibitors, even at the highest concentrations tested, although the remaining parasites were small in size (Figure S4B).

Hybrid Capture Reveals *P. vivax* Hypnozoite Transcriptome in the MPCCs

To further characterize the hypnozoite stage at a molecular level, we performed RNA-seq on hypnozoite-enriched MPCC cultures on day 9 post-infection. Hypnozoite enrichment was achieved by treatment with a PI4K inhibitor in "radical cure" mode and processed in parallel with untreated cultures (referred to as mixed samples) (Figure 4A). Total RNA from infected MPCCs was prepared and enriched for *P. vivax* transcripts by magnetic pull-down using custom made baits tiling the recently assembled *P. vivax* P01 genome (Auburn et al., 2016). Baits were designed to include all *P. vivax* annotated genes and intergenic regions, and exclude rRNA transcripts and regions with homology to human or mouse. Selection by hybrid capture was followed by Illumina HiSeq 2000 sequencing to generate over 100 million single-end 40 nt reads, with an average of 29 million reads per sample (Figure 4B). Alignment to *P. vivax* P01 transcriptome revealed robust enrichment, with approximately 92% and 48% of reads mapping uniquely to *P. vivax* in mixed and hypnozoite-enriched cultures, respectively (Table S1; Figures S5 and S6). Notably, hypnozoite-enriched samples showed lower library complexity compared to mixed samples, suggestive of a preserved, albeit reduced transcriptional activity, consistent with a quiescent state (Figure 4C).

Hypnozoite-enriched samples showed a significantly different transcriptional profile relative to mixed samples (Figure 4E). Gene ontology (GO) enrichment analysis of the differentially

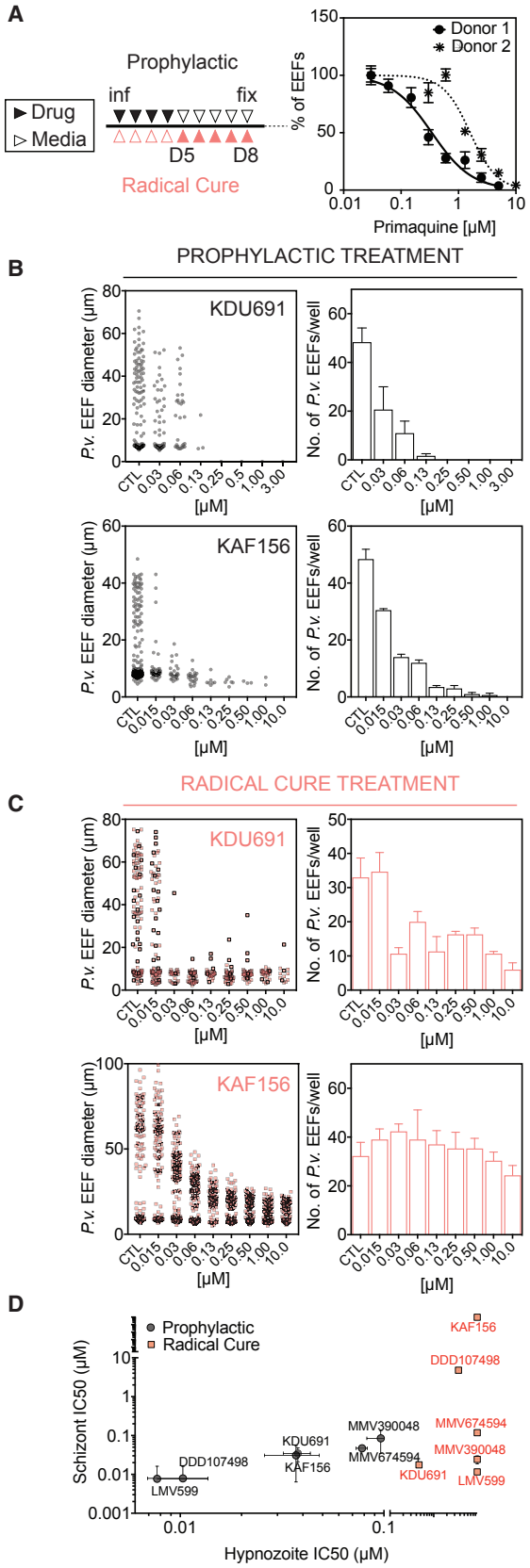

Figure 3. *In vitro* Hypnozoites Serve as an Antimalarial Testing Platform

(A) Left: representative dosing regimens for the drugs tested. Drug is added to cultures (filled triangles), or cultures are kept with daily drug-free media changes (open triangles). Prophylactic dosing begins 3 hpi (black); radical cure dosing begins 5 days pi (red). Right: prophylactic PQ dosing. PHHs with different CYP2D6 activities were used to create MPCCs that were infected with the same *P. vivax* clinical isolate (VK210). IC_{50} curves were produced by plotting fraction of EEFs remaining in culture at each concentration, as measured against untreated control wells (mean ± SEM, n = 3, two donors were tested in three independent experiments). Donor 1 is used for all subsequent experiments.

(B) KDU691 and KAF156 were dosed following the prophylactic regimen in (A), and on day 8, the diameter and number of remaining EEFs were assayed (mean ± SEM, n = 3).

(C) KDU691 and KAF156 were dosed following the radical cure regimen in (A), and on day 8, the diameter and number of remaining EEFs were assayed (mean ± SEM, n = 3).

(D) IC_{50} values of six compounds in prophylactic and radical cure modes (mean ± SEM, n = 3). Break in axes indicate highest concentration tested. See also Figure S4B.

expressed genes revealed suppression of functions related to maturity, merozoite invasion, and egress in the hypnozoite-enriched samples (Table S1). We also found that regulators of transcription, namely, members of the plant-derived Apicomplexan Apetala2 (ApiAP2) family of transcription factors (Balaji et al., 2005) were altered in the two populations (Figure 4D; Table S1). In one example, PVP01_1016100 (AP2-Q), which has been proposed as a quiescence marker in *P. cynomolgi* (Cubi et al., 2017), exhibited low representation in both mixed and hypnozoite-enriched samples (transcripts per million [TPM] < 25). Another AP2-encoding gene, PVP01_0916300, was observed at higher transcript abundance (TPM > 150) and showed significantly higher representation in hypnozoite-enriched samples. Notably, the liver-specific AP2, PVP01_0216000 (Iwanaga et al., 2012) had equivalent representation in the two sample sets (TPM > 160). Relative abundance of these transcripts, as well as transcripts of a subset of genes in the identified GO terms were confirmed by performing qRT-PCR on the same RNA samples prior to hybrid selection, as well as on independently collected samples (Figure 4F).

Finally, to evaluate the potential to apply insights from the transcriptome data toward drug discovery efforts, we mined the datasets for relative expression of several known drug targets. For the compounds tested against hypnozoites in MPCCs (Figure 3D), two targets have been identified: PI4K (McNamara et al., 2013) and eEF2 (Baragaña et al., 2015). Hybrid capture and qRT-PCR analysis showed lower representation of genes coding for PI4K and eEF2 in hypnozoite-enriched samples relative to mixed samples (Figures 4D and 4E), which could explain the superior killing activity of the four PI4K inhibitors and DDD107498 on schizonts versus hypnozoites under radical cure treatment (Figure 3). However, we cannot exclude the possibility that the experimental framework selected for drug-insensitive hypnozoites, nor that the target pathway was downregulated in response to drug treatment.

MPCCs Can Be Fabricated in 384-Well Plates

Anti-hypnozoite drug screening efforts can be improved by reducing biomass requirements, since access to sporozoites is

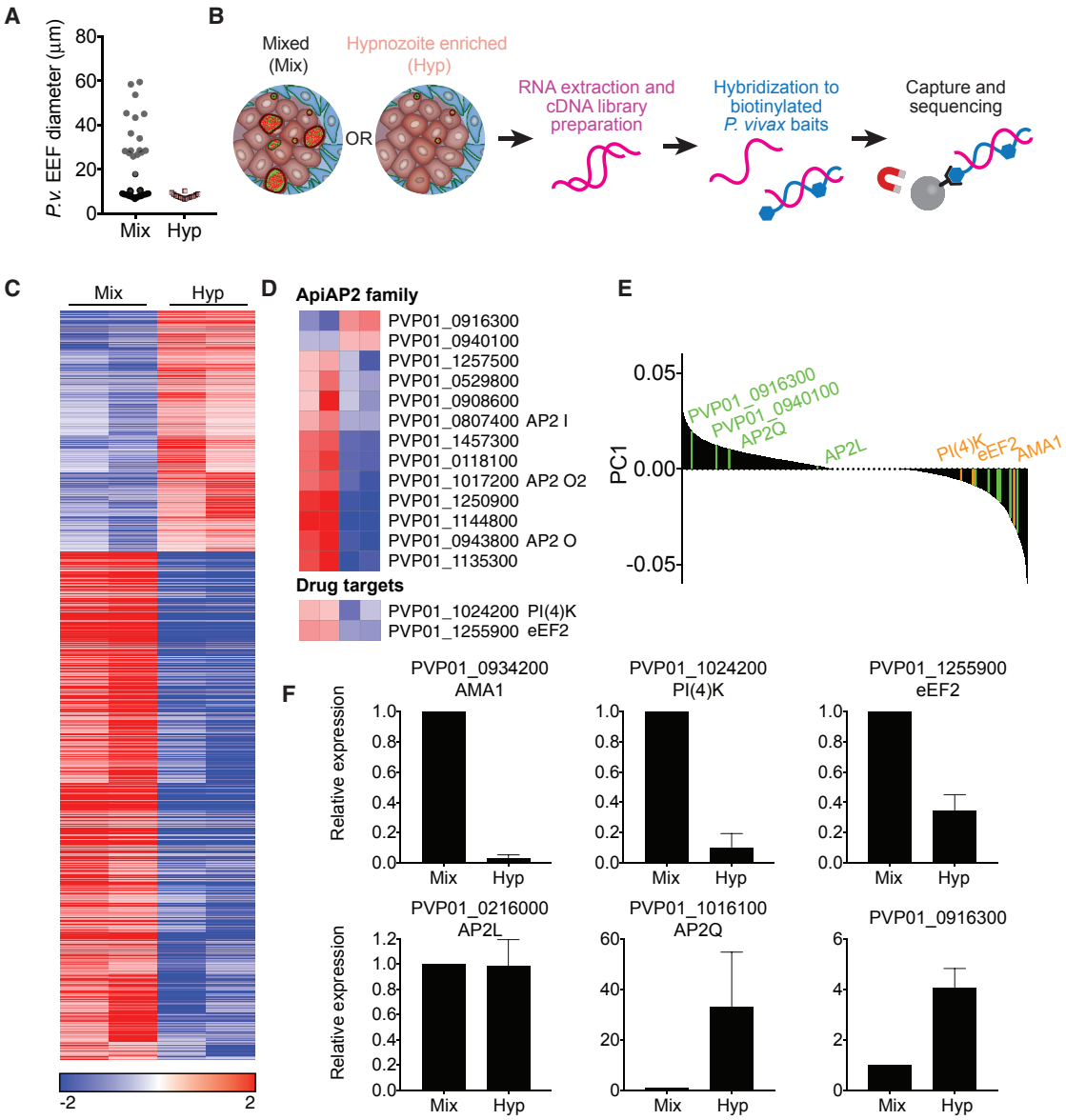

Figure 4. RNA-Seq Reveals Differential Expression Patterns between Hypnozoites and Schizonts

(A) Cultures were treated with a PI4K inhibitor in radical cure mode to enrich for hypnozoites. Drug was removed on day 8 pi and cultures were kept for 1 additional day in media before processing. Diameters of EEFs remaining in culture on day 9 were plotted for treated and untreated cultures.

(B) Schematic of sample processing. RNA extraction was performed on mixed and hypnozoite-enriched cultures on day 9. cDNA libraries were hybridized to *P. vivax*-specific baits for enrichment before sequencing.

(C) Heatmap was generated for transcripts with adjusted p value (padj) < 0.01. Median log-transformed TPM values were calculated for each gene and the log2 fold changes over the median was calculated for each sample. The resulting matrix was subjected to hierarchical clustering (two biological replicates per condition).

(D) Top heatmap shows differential representation of ApiAP2 genes in mixed versus hypnozoite-enriched samples (padj < 0.01). Bottom heatmap shows differential representation of drug targets PI4K and eEF2.

(E) Principal component analysis where positive values are biased toward hypnozoite-enriched samples. Genes in the ApiAP2 family are indicated in green and additional genes for which qRT-PCR analysis was performed are indicated in orange.

(F) qRT-PCR analysis of five representative genes in non-captured RNA samples (mean ± SEM from at least three biological replicates of which one is an independent sample, not used for hybrid selection).

a major logistical bottleneck. Toward this goal, we scaled down the MPCC platform to be compatible with industry standard 384-well plates. We have previously shown that precise ratios of homotypic and heterotypic interactions play essential roles in maintaining hepatocyte function in MPCCs (Khetani and Bhatia, 2008). In line with this observation, adapting the protocol for use in the smaller, 384-well system required that the island size and center-to-center distances were preserved. The

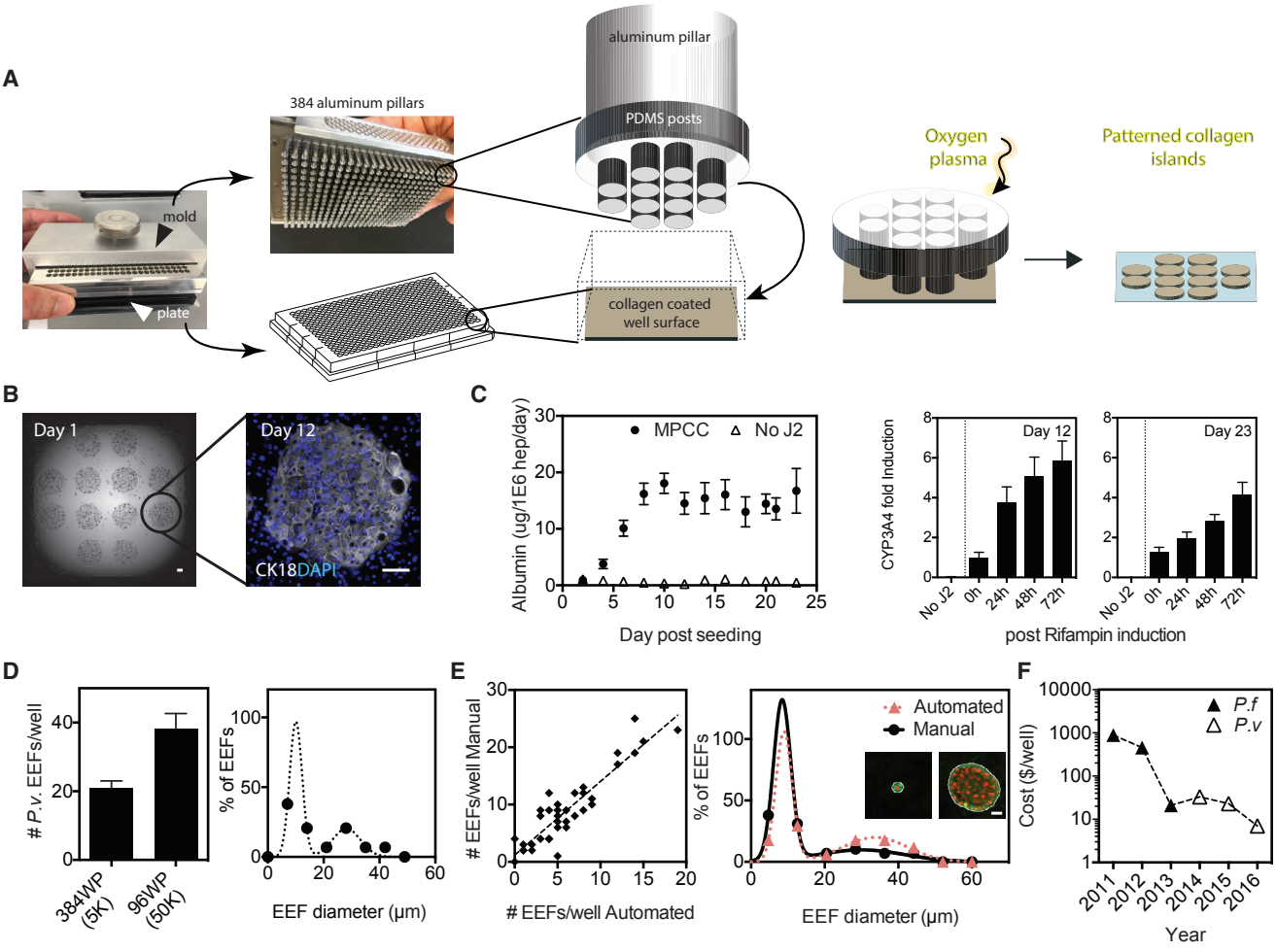

Figure 5. *P. vivax*-Infected MPCCs Are Reengineered in 384-Well Plates

(A) Images of the 384-well plate MPCC mold and schematics describing the collagen ablation process.

(B) Representative image of PHHs seeded on collagen islands in a 384-well plate on day 1, before addition of fibroblasts (left panel). Representative image of CK18 expression on day 12 (right panel). Scale bars, 100 μm.

(C) Albumin levels in PHHs with (MPCC) and without fibroblast (no J2) for at least 3 weeks in culture (left panel). CYP3A4 activity assay post-rifampin treatment on days 12 and 23 (middle and right panels).

(D) Comparison of infection rates in 384 and 96 MPCCs. Sporozoite doses are indicated in parentheses. Histogram of day 8 forms in 384 MPCCs (right panel).

(E) Comparison of EEF numbers (n = 36) and sizes (n = 5) according to manual or automated image analysis. Inset shows a representative hypnozoite and schizont with white outline detected by the algorithm to measure size. Scale bar, 10 μm.

(F) MPCC cost reduction, including PHHs, sporozoites, chemical screening, reagents, imaging, and labor (2016: switch to 384 MPCCs).

monolithic (poly)dimethylsiloxane (PDMS) mold with elastomeric pillars and patterns was re-designed and precision-engineered to be compatible with the 384-well plate format. The 384-mold consists of individually spring loaded, composite metal-PDMS pillars with protruding patterns. The protruding patterns comprise 12 soft PDMS posts that, when in contact with the collagen-coated surface of each well, protect islands of collagen from ablation when exposed to oxygen plasma (Figure 5A). Spring-loading each pillar ensures uniform, conformal contact across an entire 384-well plate. After plasma treatment, seeded PHHs selectively attach to the remaining collagen pattern and are subsequently surrounded by supportive stromal cells.

Seeded PHHs, positive for host markers such as CK18 (Figure 5B), were functionally stable for 3 weeks, as depicted via stable albumin secretion levels. Furthermore, a primary drug metabolism enzyme, CYP3A4, remained both active and inducible for at least 23 days (Figure 5C). A pilot infection of the 384 MPCCs with clinical Thai *P. vivax* isolates revealed only a 2-fold reduction in infection rates per well compared with the 96-well format, despite the 10-fold reduction in initial parasite load and a 3-fold reduction in number of PHHs seeded. When expressed as a function of infection efficiency, this encouraging proof-of-concept translates to an enhanced outcome per biomass of 1.5-fold (hepatocytes), or 5-fold (parasites). On day 8, a bimodal population in parasite size became apparent, allowing distinction of hypnozoites and schizonts (Figure 5D). Furthermore, the platform is fully automatable. Cell seeding, media change, and drug-dosing steps can be performed with liquid

handlers; imaging with an automated microscope; and image analysis using Cell Profiler (Carpenter et al., 2006; Jones et al., 2008). In one example, automated imaging and subsequent Cell Profiler analysis revealed strong agreement between automated and manual parasite counts and sizes, suitable for high-throughput drug screening (Figure 5E). Finally, we have achieved a 200× reduction in the cost per well of the MPCC platform since 2011 for antimalarial screen purposes (Figure 5F). The decreased biomass needs achieved by the 384 MPCC represents the most significant contributor to the price reduction in 2016.

DISCUSSION

This study presents a rigorous *in vitro* characterization of hypnozoites, including assessment of their functional hallmarks and transcriptional profile. Hypnozoites detected in the MPCC system exhibit the known hallmarks of this liver stage: they are small, uninucleate, MSP1-negative, and differentially sensitive to primaquine versus atovoquone. Furthermore, in addition to persistent hypnozoites, we also observe large forms that re-emerge on day 21, consistent with potential reactivation.

The demonstrated capacity to culture hypnozoites marks the MPCC system as a promising screening platform (in 96- and 384-well formats), and paves the way toward high-throughput testing of existing and novel antimalarial candidates. Drug testing can be performed in both prophylactic and radical cure dosing strategies that target growing liver-stage parasites or established hypnozoites, respectively (Campo et al., 2015). Here, we tested six compounds: KAF156, DDD107798 and four compounds that target PI4K. All six compounds cleared both hypnozoites and schizonts under prophylactic treatment. Under radical cure treatment, some of the drugs had killing activity against large forms, but were unable to eliminate remaining small forms. This observation is in line with relapses reported in monkeys treated with the same compounds (Zeeman et al., 2016), demonstrating the predictive capacity of MPCCs in both prophylactic and radical cure dosing regimens. Notably, this screening platform offers the added benefit of using *P. vivax* as the test parasite, without the need for large animal studies. For more thorough characterization of the remaining small forms under drug pressure, long-term kinetic studies should be performed to measure their reactivation capacity.

Primaquine remains the only clinically approved drug with anti-hypnozoite activity. It should be noted that while, to the best of our knowledge, the MPCC system is the only *in vitro* system that has shown elimination of *P. vivax* parasites with prophylactic primaquine treatment, the radical cure treatment regimen used here has not achieved complete clearance of small forms as assessed by microscopy. The clinical standard of primaquine radical cure requires a 14-day regimen, usually co-administered with chloroquine, with blood-stage breakthrough as a readout. However, clinical studies show that even with this dosing regimen, relapses occur in individuals infected with *P. vivax*, likely due to inadequate dosing, geographical origin of the parasite, evolving primaquine resistance, or a combination of these factors (Collins and Jeffery, 1996; Goller et al., 2007). It is possible that radical cure *in vitro* might require a longer dosing regimen, in combination with a blood schizonticide. Furthermore, the observed lack of primaquine efficacy from day 5 cultures onward raises questions regarding the biological changes that the hypnozoite might undergo. Given that the mechanism of hypnozoite clearance in the human liver has not yet been identified, to definitively assess whether the remaining small forms observed in culture post-treatment are viable parasites, their reactivation capacity should be interrogated with longer-term studies, combined with reticulocyte overlays to assess blood breakthrough.

Toward further molecular characterization of the elusive dormant parasites, we provide here the *P. vivax* hypnozoite transcriptome. This was achieved via a hybrid capture method whereby parasite transcripts were enriched using nucleic acid "baits" designed specifically for the *P. vivax* genome. While a similar strategy has previously been used to enrich for pathogen DNA in clinical blood samples (Melnikov et al., 2011), here we apply hybrid selection for RNA enrichment of low input samples prior to sequencing. The obtained results were successfully corroborated by an independent method (RT-PCR), for various targets in multiple samples, strengthening confidence in our findings. This new methodology can now be applied toward querying transcriptomes of not only *Plasmodium* liver stages, but also other developmental stages of the parasite in mammalian and mosquito hosts, which have historically been challenging to perform due to major host contamination. We anticipate the utility of this tool toward elucidating the dynamic transcriptomes of the full parasite life cycle, identifying stage-specific biomarkers, as well as elucidating novel drug and vaccine targets.

RNA capture and sequencing described here demonstrated that *P. vivax* hypnozoites exhibit reduced transcriptional activity, with low numbers of transcripts showing relatively high representation compared with the schizont stage. While 40% of the identified transcripts encode proteins of unknown function, the gene list contains RNA and DNA binding proteins, nucleases, proteases, and transferases, suggestive of preserved metabolic and catalytic activity, which could be linked to the observed increase in hypnozoite size in our long-term cultures. Consistent with a recent transcriptomic study of *P. cycnomolgi* hypnozoites, we also found members of the ApiAP2 family of transcription factors represented in hypnozoite-enriched samples. In addition to AP2Q, which was proposed as a transcriptional suppressor (but showed fairly low representation and high variation in our *P. vivax* samples), we identified a second putative AP2, PVP01_0916300 with more robust representation. PVP01_0916300 appears to also be highly expressed in *P. falciparum* gametocytes (López-Barragán et al., 2011), another quiescent form of the parasite. It would be interesting to investigate whether different quiescent parasite stages share similar regulatory mechanisms. ApiAP2 factors have been shown to regulate stage-specific transcription and parasite development (Iwanaga et al., 2012; Kafsack et al., 2014; Modrzynska et al., 2017; Sinha et al., 2014; Yuda et al., 2009, 2010), and thus are attractive candidates for further investigation and validation as regulators of the quiescent state. Notably, there are several putative AP2s that showed higher representation in mixed cultures and may be important as transcription activators, or even implicated in reactivation. One example that could be of interest to investigate is PVP01_0118100, which is one of the 25% of differentially

detected genes that are exclusively found in *P. vivax*, *P. cynomolgi*, *P. fragile*, *P. knowlesi*, and *P. inui*, with no orthologs in *P. falciparum* or rodent malaria parasites. Other unveiled candidates for which no function has been assigned could also be explored in the future as hypnozoite-specific biomarkers.

Finally, hypnozoite-specific properties of *P. vivax* infections, that have so far been observed largely in clinical studies, can be investigated in MPCCs. *P. vivax* strains that originate from different regions of the world are known to give rise to different relapse frequencies (Battle et al., 2014; Goller et al., 2007), which has been attributed to varying hypnozoite ratios (White, 2011). Recently, one study compared the two Thai isolate CSP subtypes using a humanized mouse system and found differences in hypnozoite frequencies (Mikolajczak et al., 2015). Our results however reveal hypnozoite frequencies ranging from 11% to 48%, regardless of the CSP subtype. It is not clear whether the VK210 and VK247 categorization of *P. vivax* is sufficient to capture hypnozoite frequency or other biological differences, if any, between the Thai strains. Future studies using parasites derived from other geographic locations should elucidate similarities and differences between strains, including drug sensitivity.

Overall, our data highlight the capacity of the MPCC system to facilitate interrogations of hypnozoite biology and testing of anti-hypnozoite compounds in the absence of dependence on human experimentation. MPCCs offer advantages over existing *in vitro* systems. The longevity of cultures allow monitoring of important *P. vivax* hallmarks such as merosome release and reactivation as well as testing of hypotheses regarding reactivation (Shanks and White, 2013); having a full repertoire of host functions allows for primaquine sensitivity and cross-screening for cellular toxicity; and its reproducibility allows drug sensitivity testing. MPCCs are compatible with robotic fluid handlers and high-content imaging readouts and are suitable for international dissemination, with training, as demonstrated by the implementation of the platform at four sites in two countries. Compared to *in vivo* systems, MPCCs enable biomass enrichment due to the well-plate format, reduced biomass requirements, and dynamic monitoring of parasite biology via microscopy, such as time-lapse longitudinal studies of live cultures. Finally, the MPCCs allow querying of the liver-stage transcriptome of *P. vivax* and will enable profiling of hypnozoite transcripts over time and in response to drug pressure. Taken together, the robust, high-throughput-ready *in vitro* human liver system presented here offers the potential to gain new biological insights into *P. vivax* development in human hepatocytes, and represents a screening platform for candidate drugs directed against distinct stages of *P. vivax*, including the hypnozoite stage, a required asset in the push to achieve malaria eradication.

STAR★METHODS

Detailed methods are provided in the online version of this paper and include the following:

- KEY RESOURCES TABLE
- CONTACT FOR REAGENT AND RESOURCE SHARING
- EXPERIMENTAL MODEL AND SUBJECT DETAILS
  - *P. vivax* Parasites
  - Cells
- METHOD DETAILS
  - Micropatterned Co-cultures (MPCCs)
  - *P. vivax* Infection of MPCCs
  - Human Reticulocyte Overlay
  - Drug Treatment of *P. vivax* EEFs in MPCCs
  - Immunofluorescence Staining
  - Hybrid Capture, RNA-seq Extraction and Analysis
  - Quantitative RT-PCR
- QUANTIFICATION AND STATISTICAL ANALYSIS
  - Sample Sizes and Statistical Analysis
  - RNA-seq Data
- DATA AND SOFTWARE AVAILABILITY
  - Raw Data

SUPPLEMENTAL INFORMATION

Supplemental Information includes six figures, two tables, and three movies and can be found with this article online at https://doi.org/10.1016/j.chom.2018.01.002.

ACKNOWLEDGMENTS

We are grateful to MMV and Kelly Chibale for supplying the compounds; Wanlapa Roobsong for help with reticulocytes; Adam Falls for assistance with the 384 MPCC mold; Sabrina Hawthorne, Owen Hardy, and the Koch Institute Swanson Biotechnology Center, specifically Jon Penterman in the Genomics Core Facility, for technical support; Maria Mota, Stephen Hoffman, Brice Campo, Omar Vandal, Richard Elliott, Dan Neafsey, Bronwyn MacInnis, Dyann Wirth, and James J. Collins for insightful discussions. This work was supported by the Bill & Melinda Gates Foundation (OPP1023607), a BN10 grant from the Broad Institute, and in part by the Koch Institute Support Grant P30-CA14051 from the National Cancer Institute. *P. vivax* sporozoite production was supported by MMV. N.G. is an HHMI International Student Research Fellow. S.N.B. is an HHMI Investigator.

AUTHOR CONTRIBUTIONS

N.G., S.M., and S.N.B. conceived the study. N.G., L.M.-S., and S.M. designed the experiments. N.G., A.B.M., L.M.-S., and A.G. performed the experiments. R.P., J.S., S.A.M., and S.H.I.K. contributed the reagents. V.L.B. and S.S.L. helped design, perform, and analyze the RNA-seq experiments. S.P.D. designed the 384 MPCC mold. The manuscript was prepared by N.G., L.M.-S., J.S., H.E.F., and S.N.B.

DECLARATION OF INTERESTS

S.N.B. is a co-founder of Ascendance, which commercially manufactures and distributes micropatterned co-cultures.

Received: July 19, 2017
Revised: November 21, 2017
Accepted: January 3, 2018
Published: February 22, 2018

REFERENCES

Anders, S., and Huber, W. (2010). Differential expression analysis for sequence count data. Genome Biol. *11*, R106.

Auburn, S., Böhme, U., Steinbiss, S., Trimarsanto, H., Hostetler, J., Sanders, M., Gao, Q., Nosten, F., Newbold, C.I., Berriman, M., et al. (2016). A new *Plasmodium vivax* reference sequence with improved assembly of the subtelomeres reveals an abundance of pir genes. Wellcome Open Res. *1*, 4.

Balaji, S., Babu, M.M., Iyer, L.M., and Aravind, L. (2005). Discovery of the principal specific transcription factors of Apicomplexa and their implication for the evolution of the AP2-integrase DNA binding domains. Nucleic Acids Res. *33*, 3994–4006.

Baragaña, B., Hallyburton, I., Lee, M.C.S., Norcross, N.R., Grimaldi, R., Otto, T.D., Proto, W.R., Blagborough, A.M., Meister, S., Wirjanata, G., et al. (2015). A novel multiple-stage antimalarial agent that inhibits protein synthesis. Nature *522*, 315–320.

Battle, K.E., Karhunen, M.S., Bhatt, S., Gething, P.W., Howes, R.E., Golding, N., Van Boeckel, T.P., Messina, J.P., Shanks, G.D., Smith, D.L., et al. (2014). Geographical variation in *Plasmodium vivax* relapse. Malar. J. *13*, 144.

Benjamini, Y., and Hochberg, Y. (1995). Controlling the false discovery rate: a practical and powerful approach to multiple testing. J. R. Stat. Soc. Ser. B *57*, 289–300.

Bennett, J.W., Pybus, B.S., Yadava, A., Tosh, D., Sousa, J.C., McCarthy, W.F., Deye, G., Melendez, V., and Ockenhouse, C.F. (2013). Primaquine failure and cytochrome P-450 2D6 in *Plasmodium vivax* malaria. N. Engl. J. Med. *369*, 1381–1382.

Berger, D.R., Ware, B.R., Davidson, M.D., Allsup, S.R., and Khetani, S.R. (2015). Enhancing the functional maturity of induced pluripotent stem cell-derived human hepatocytes by controlled presentation of cell-cell interactions *in vitro*. Hepatology *61*, 1370–1381.

Campo, B., Vandal, O., Wesche, D.L., and Burrows, J.N. (2015). Killing the hypnozoite - drug discovery approaches to prevent relapse in *Plasmodium vivax*. Pathog. Glob. Health *109*, 107–122.

Carpenter, A.E., Jones, T.R., Lamprecht, M.R., Clarke, C., Kang, I., Friman, O., Guertin, D.A., Chang, J., Lindquist, R.A., Moffat, J., et al. (2006). CellProfiler: image analysis software for identifying and quantifying cell phenotypes. Genome Biol. *7*, R100.

Chattopadhyay, R., Velmurugan, S., Chakiath, C., Andrews Donkor, L., Milhous, W., Barnwell, J.W., Collins, W.E., and Hoffman, S.L. (2010). Establishment of an in vitro assay for assessing the effects of drugs on the liver stages of *Plasmodium vivax* malaria. PLoS One *5*, e14275.

Collins, W.E., and Jeffery, G.M. (1996). Primaquine resistance in *Plasmodium vivax*. Am. J. Trop. Med. Hyg. *55*, 243–249.

Combe, A., Giovannini, D., Carvalho, T.G., Spath, S., Boisson, B., Loussert, C., Thiberge, S., Lacroix, C., Gueirard, P., and Ménard, R. (2009). Clonal conditional mutagenesis in malaria parasites. Cell Host Microbe *5*, 386–396.

Cubi, R., Vembar, S.S., Biton, A., Franetich, J.-F., Bordessoulles, M., Sossau, D., Zanghi, G., Bosson-Vanga, H., Benard, M., Moreno, A., et al. (2017). Laser capture microdissection enables transcriptomic analysis of dividing and quiescent liver stages of *Plasmodium* relapsing species. Cell. Microbiol. *19*, e12735.

Dembele, L., Gego, A., Zeeman, A.-M., Franetich, J.-F., Silvie, O., Rametti, A., Le Grand, R., Dereuddre-Bosquet, N., Sauerwein, R., van Gemert, G.-J., et al. (2011). Towards an in vitro model of *Plasmodium* hypnozoites suitable for drug discovery. PLoS One *6*, e18162.

Dobin, A., Davis, C.A., Schlesinger, F., Drenkow, J., Zaleski, C., Jha, S., Batut, P., Chaisson, M., and Gingeras, T.R. (2013). STAR: ultrafast universal RNA-seq aligner. Bioinformatics *29*, 15–21.

Ghidelli-Disse, S., Lafuente-Monasterio, M., Waterson, D., Witty, M., Younis, Y., Paquet, T., Street, L.J., Chibale, K., Gamo-Benito, F., Bantscheff, M., et al. (2014). Identification of *Plasmodium* PI4 kinase as target of MMV390048 by chemoproteomics. Malar. J. *13*, P38.

Goller, J.L., Jolley, D., Ringwald, P., and Biggs, B.-A. (2007). Regional differences in the response of *Plasmodium vivax* malaria to primaquine as antirelapse therapy. Am. J. Trop. Med. Hyg. *76*, 203–207.

Gural, N., Mancio-Silva, L., He, J., and Bhatia, S.N. (2018). Engineered Livers for Infectious Diseases. Cell. Mol. Gastroenterol. Hepatol. *5*, 131–144.

Hollingdale, M.R., Collins, W.E., Campbell, C., and Schwartz, A.L. (1985). In vitro culture of two populations (dividing and nondividing) of exoerythrocytic parasites of *Plasmodium vivax*. Am. J. Trop. Med. Hyg. *34*, 216–222.

Iwanaga, S., Kaneko, I., Kato, T., and Yuda, M. (2012). Identification of an AP2-family protein that is critical for malaria liver stage development. PLoS One *7*, e47557.

Jones, T.R., Kang, I., Wheeler, D.B., Lindquist, R.A., Papallo, A., Sabatini, D.M., Golland, P., and Carpenter, A.E. (2008). CellProfiler Analyst: data exploration and analysis software for complex image-based screens. BMC Bioinformatics *9*, 482.

Kafsack, B.F.C., Rovira-Graells, N., Clark, T.G., Bancells, C., Crowley, V.M., Campino, S.G., Williams, A.E., Drought, L.G., Kwiatkowski, D.P., Baker, D.A., et al. (2014). A transcriptional switch underlies commitment to sexual development in malaria parasites. Nature *507*, 248–252.

Kaplowitz, N. (2005). Idiosyncratic drug hepatotoxicity. Nat. Rev. Drug Discov. *4*, 489–499.

Khetani, S.R., and Bhatia, S.N. (2008). Microscale culture of human liver cells for drug development. Nat. Biotechnol. *26*, 120–126.

Krotoski, W.A., Krotoski, D.M., Garnham, P.C., Bray, R.S., Killick-Kendrick, R., Draper, C.C., Targett, G.A., and Guy, M.W. (1980). Relapses in primate malaria: discovery of two populations of exoerythrocytic stages. Preliminary note. Br. Med. J. *280*, 153–154.

Krotoski, W.A., Collins, W.E., Bray, R.S., Garnham, P.C., Cogswell, F.B., Gwadz, R.W., Killick-Kendrick, R., Wolf, R., Sinden, R., Koontz, L.C., et al. (1982). Demonstration of hypnozoites in sporozoite-transmitted *Plasmodium vivax* infection. Am. J. Trop. Med. Hyg. *31*, 1291–1293.

Kuhen, K.L., Chatterjee, A.K., Rottmann, M., Gagaring, K., Borboa, R., Buenviaje, J., Chen, Z., Francek, C., Wu, T., Nagle, A., et al. (2014). KAF156 is an antimalarial clinical candidate with potential for use in prophylaxis, treatment, and prevention of disease transmission. Antimicrob. Agents Chemother. *58*, 5060–5067.

Li, B., and Dewey, C.N. (2011). RSEM: accurate transcript quantification from RNA-Seq data with or without a reference genome. BMC Bioinformatics *12*, 323.

López-Barragán, M.J., Lemieux, J., Quiñones, M., Williamson, K.C., Molina-Cruz, A., Cui, K., Barillas-Mury, C., Zhao, K., and Su, X. (2011). Directional gene expression and antisense transcripts in sexual and asexual stages of *Plasmodium falciparum*. BMC Genomics *12*, 587.

Love, M.I., Huber, W., and Anders, S. (2014). Moderated estimation of fold change and dispersion for RNA-seq data with DESeq2. Genome Biol. *15*, 550.

March, S., Ramanan, V., Trehan, K., Ng, S., Galstian, A., Gural, N., Scull, M.A., Shlomai, A., Mota, M.M., Fleming, H.E., et al. (2015). Micropatterned coculture of primary human hepatocytes and supportive cells for the study of hepatotropic pathogens. Nat. Protoc. *10*, 2027–2053.

Mazier, D., Landau, I., Druilhe, P., Miltgen, F., Guguen-Guillouzo, C., Baccam, D., Baxter, J., Chigot, J.-P., and Gentilini, M. (1984). Cultivation of the liver forms of *Plasmodium vivax* in human hepatocytes. Nature *307*, 367–369.

McNamara, C.W., Lee, M.C.S., Lim, C.S., Lim, S.H., Roland, J., Nagle, A., Simon, O., Yeung, B.K.S., Chatterjee, A.K., McCormack, S.L., et al. (2013). Targeting *Plasmodium* PI(4)K to eliminate malaria. Nature *504*, 248–253.

Melnikov, A., Galinsky, K., Rogov, P., Fennell, T., Van Tyne, D., Russ, C., Daniels, R., Barnes, K.G., Bochicchio, J., Ndiaye, D., et al. (2011). Hybrid selection for sequencing pathogen genomes from clinical samples. Genome Biol. *12*, R73.

Mikolajczak, S.A., Vaughan, A.M., Kangwanrangsan, N., Roobsoong, W., Fishbaugher, M., Yimamnuaychok, N., Rezakhani, N., Lakshmanan, V., Singh, N., Kaushansky, A., et al. (2015). *Plasmodium vivax* liver stage development and hypnozoite persistence in human liver-chimeric mice. Cell Host Microbe *17*, 526–535.

Miller, J.L., Harupa, A., Kappe, S.H.I., and Mikolajczak, S.A. (2012). *Plasmodium yoelii* macrophage migration inhibitory factor is necessary for efficient liver-stage development. Infect. Immun. *80*, 1399–1407.

Modrzynska, K., Pfander, C., Chappell, L., Yu, L., Suarez, C., Dundas, K., Gomes, A.R., Goulding, D., Rayner, J.C., Choudhary, J., et al. (2017). A knockout screen of ApiAP2 genes reveals networks of interacting transcriptional regulators controlling the plasmodium life cycle. Cell Host Microbe *21*, 11–22.

Ng, S., Schwartz, R.E., March, S., Galstian, A., Gural, N., Shan, J., Prabhu, M., Mota, M.M., and Bhatia, S.N. (2015). Human iPSC-derived hepatocyte-like cells support plasmodium liver-stage infection in vitro. Stem Cell Reports *4*, 348–359.

Noe, A.R., Fishkind, D.J., and Adams, J.H. (2000). Spatial and temporal dynamics of the secretory pathway during differentiation of the *Plasmodium yoelii* schizont. Mol. Biochem. Parasitol. *108*, 169–185.

Ploss, A., Khetani, S.R., Jones, C.T., Syder, A.J., Trehan, K., Gaysinskaya, V.A., Mu, K., Ritola, K., Rice, C.M., and Bhatia, S.N. (2010). Persistent hepatitis C virus infection in microscale primary human hepatocyte cultures. Proc. Natl. Acad. Sci. USA *107*, 3141–3145.

Price, R.N., von Seidlein, L., Valecha, N., Nosten, F., Baird, J.K., and White, N.J. (2014). Global extent of chloroquine-resistant *Plasmodium vivax*: a systematic review and meta-analysis. Lancet Infect. Dis. *14*, 982–991.

Rosenberg, R., Wirtz, R.A., Lanar, D.E., Sattabongkot, J., Hall, T., Waters, A.P., and Prasittisuk, C. (1989). Circumsporozoite protein heterogeneity in the human malaria parasite *Plasmodium vivax*. Science *245*, 973–976.

Sattabongkot, J., Yimamnuaychoke, N., Leelaudomlipi, S., Rasameesoraj, M., Jenwithisuk, R., Coleman, R.E., Udomsangpetch, R., Cui, L., and Brewer, T.G. (2006). Establishment of a human hepatocyte line that supports in vitro development of the exo-erythrocytic stages of the malaria parasites *Plasmodium falciparum* and *P. vivax*. Am. J. Trop. Med. Hyg. *74*, 708–715.

Shanks, G.D., and White, N.J. (2013). The activation of vivax malaria hypnozoites by infectious diseases. Lancet Infect. Dis. *13*, 900–906.

Shortt, H.E., and Garnham, P.C.C. (1948). Pre-erythrocytic stage in mammalian malaria parasites. Nature *161*, 126.

Sinha, A., Hughes, K.R., Modrzynska, K.K., Otto, T.D., Pfander, C., Dickens, N.J., Religa, A.A., Bushell, E., Graham, A.L., Cameron, R., et al. (2014). A cascade of DNA-binding proteins for sexual commitment and development in *Plasmodium*. Nature *507*, 253–257.

Sturm, A., Amino, R., van de Sand, C., Regen, T., Retzlaff, S., Rennenberg, A., Krueger, A., Pollok, J.-M., Menard, R., and Heussler, V.T. (2006). Manipulation of host hepatocytes by the malaria parasite for delivery into liver sinusoids. Science *313*, 1287–1290.

Wells, T.N.C., Burrows, J.N., and Baird, J.K. (2010). Targeting the hypnozoite reservoir of *Plasmodium vivax*: the hidden obstacle to malaria elimination. Trends Parasitol. *26*, 145–151.

White, N.J. (2011). Determinants of relapse periodicity in *Plasmodium vivax* malaria. Malar. J. *10*, 297.

WHO. (2015). World Malaria Report 2015 (World Health Organization).

Younis, Y., Douelle, F., Feng, T.S., González Cabrera, D., Le Manach, C., Nchinda, A.T., Duffy, S., White, K.L., Shackleford, D.M., Morizzi, J., et al. (2012). 3,5-Diaryl-2-aminopyridines as a novel class of orally active antimalarials demonstrating single dose cure in mice and clinical candidate potential. J. Med. Chem. *55*, 3479–3487.

Yuda, M., Iwanaga, S., Shigenobu, S., Mair, G.R., Janse, C.J., Waters, A.P., Kato, T., and Kaneko, I. (2009). Identification of a transcription factor in the mosquito-invasive stage of malaria parasites. Mol. Microbiol. *71*, 1402–1414.

Yuda, M., Iwanaga, S., Shigenobu, S., Kato, T., and Kaneko, I. (2010). Transcription factor AP2-Sp and its target genes in malarial sporozoites. Mol. Microbiol. *75*, 854–863.

Zeeman, A.-M., Lakshminarayana, S.B., van der Werff, N., Klooster, E.J., Voorberg-van der Wel, A., Kondreddi, R.R., Bodenreider, C., Simon, O., Sauerwein, R., Yeung, B.K.S., et al. (2016). PI4K is a prophylactic, but not radical curative target in *Plasmodium vivax*-type malaria parasites. Antimicrob. Agents Chemother. *60*, AAC.03080–15.

STAR★METHODS

KEY RESOURCES TABLE

REAGENT or RESOURCE	SOURCE	IDENTIFIER
Antibodies		
Alexa 546-conjugated secondary goat-anti-mouse	Invitrogen	Cat# A11030; RRID: AB_144695
Alexa 647-conjugated goat anti-rabbit	Invitrogen	Cat# A21246; RRID: AB_1500778
Hoechst 33258	Invitrogen	Cat# H3569; RRID: AB_2651133
rabbit polyclonal anti-acetyl-Histone H3 (Lys9) antibody	Millipore	Cat# 06-942; RRID: AB_310308
rabbit polyclonal UIS4 antibody	gift from Sebastian Mikolajcak at CIDR	N/A
rabbit polyclonal BIP antibody	gift from Sebastian Mikolajcak at CIDR	N/A
rabbit polyclonal MIF antibody	gift from Sebastian Mikolajcak at CIDR	N/A
rabbit polyclonal HSP60 antibody	gift from Sebastian Mikolajcak at CIDR	N/A
rabbit polyclonal HSP70 antibody	gift from Sebastian Mikolajcak at CIDR	N/A
rabbit polyclonal MSP1 antibody	gift from Sebastian Mikolajcak at CIDR	N/A
mouse monoclonal UIS4 antibody	gift from Sebastian Mikolajcak at CIDR	N/A
mouse monoclonal ACP antibody	gift from Sebastian Mikolajcak at CIDR	N/A
Biological Samples		
Human reticulocytes	Thai Red Cross	N/A
Primary Human Hepatocytes	Thermo Fisher, Bioreclamation IVT	N/A
Chemicals, Peptides, and Recombinant Proteins		
Aquamount	Lerner Laboratories	Cat# 41799-008
Primaquine diphosphate	Sigma	Cat# 160393
Atovaquone	Sigma	Cat# A7986
MMV67494 KDU691, LMV599, KAF156, DDD107498	Medicines for Malaria Venture	N/A
Critical Commercial Assays		
TRIzol	Thermo Fisher	Cat# 15596026
RNeasy MinElute Cleanup Kit	Qiagen	Cat# 74204
Super Script II	Thermo Fisher	Cat# 18064014
PowerUp SYBR Green Master Mix	Applied Biosystems	Cat# A25741
SureSelectXT RNA	Agilent	Custom made
Deposited Data		
Raw RNA-seq data	This paper	GEO: GSE108016)
Experimental Models: Cell Lines		
3T3-J2 murine embryonic fibroblasts	gift of Howard Green, Harvard Medical School	N/A
Experimental Models: Organisms/Strains		
Plasmodium vivax	Mahidol Vivax Research Unit (Bangkok, Thailand)	N/A
Oligonucleotides		
Primers included in Table S2	Integrated DNA Technologies	N/A
Software and Algorithms		
Illumina Offline BaseCaller v1.9.3	Illumina	N/A
STAR v. 2.5.3a	Github	https://github.com/alexdobin/STAR/releases
RSEM v. 1.3.0	Dewey Lab	https://deweylab.github.io/RSEM/
GraphPad Prism 7	GraphPad	https://www.graphpad.com/scientific-software/prism/

CONTACT FOR REAGENT AND RESOURCE SHARING

Further information and requests for resources and reagents should be directed to and will be fulfilled by the Lead Contact, Sangeeta N. Bhatia (sbhatia@mit.edu).

EXPERIMENTAL MODEL AND SUBJECT DETAILS

P. vivax Parasites

Anopheles dirus mosquitoes were fed on blood collected from symptomatic patients attending malaria clinics in Tak, Songkla, and Ubon-Ratchathani Provinces in Thailand, confirmed positive for only *P. vivax* via microscopy and RT-PCR.

Briefly, *P. vivax* infected blood was drawn into heparinized tubes and kept at 37C until processing. Infected blood was washed once with RPMI 1640 incomplete medium. Packed infected blood was resuspended in warm non-heat inactivated naïve human AB serum for a final hematocrit of 50%. Resuspended blood was fed to laboratory reared female *Anopheles dirus* mosquitoes for 30 minutes via an artificial membrane attached to a water-jacketed glass feeder kept at 37C. Engorged mosquitoes were kept on 10% sugar at 26C under 80% humidity at the designated insectary at the Mahidol Vivax Research Unit for 14 days. The confirmation of single species of *P. vivax* infection was performed by nested-PCR. Sporozoites were aseptically dissected from the salivary glands of infected mosquitoes 14–21 days after blood feeding and pooled in harvesting medium (DMEM media supplemented with 2% (v/v) penicillin-streptomycin).

Cells

Cryopreserved primary human hepatocytes were purchased from vendors permitted to sell products derived from human organs procured in the United States by federally designated Organ Procurement Organizations. Vendors include Bioreclamation IVT and Thermo Fisher. Human hepatocytes (Donor 1: female age 35; donor 2: female age 77) were maintained in high glucose Dulbecco's Modified Eagle's Medium (DMEM with L-glutamine, Corning) with 10% (v/v) fetal bovine serum (FBS, Gibco), 1% (v/v) ITS+ (insulin/human transferrin/selenous acid and linoleic acid) premix (BD Biosciences), 7 ng/ml glucagon (Sigma), 40 ng/ml dexamethasone (Sigma), 15 mM HEPES (Gibco), and 1% (v/v) penicillin-streptomycin (Corning).

J2-3T3 male murine embryonic fibroblasts (gift of Howard Green, Harvard Medical School) were cultured at <18 passages in fibroblast medium comprising of DMEM with high glucose, 10% (v/v) bovine serum (Thermo Fisher), and 1% (v/v) penicillin-streptomycin (Corning).

METHOD DETAILS

Micropatterned Co-cultures (MPCCs)

The technique has been previously explained in detail (March et al., 2015). Briefly; glass-bottomed 96 or 384-well plates were coated with rat-tail type I collagen (50 μg/ml) and subjected to soft lithographic techniques (Ploss et al., 2010) to pattern the collagen into microdomains (islands of 500 μm) that mediate selective hepatocyte adhesion. The mold for the 384MPCC was designed and constructed by Phenomyx (PHYX.384.MPCC, Cambridge, MA). Briefly, the system comprises composite aluminum-PDMS pillars with 12 circular protruding patterns arranged on an orthogonal grid. Each pillar is oriented in a polycarbonate plate and spring-loaded to ensure conformal contact with the plate bottom. A clamping plate with plasma access holes holds the 384-pillar assembly together. A sliding bracket with torque-control knob applies controlled pressure to the 384-pillar assembly during plasma ablation. To create MPCCs, cryopreserved primary human hepatocytes (Bioreclamation IVT) were pelleted by centrifugation and then seeded on collagen-micropatterned plates. 3T3-J2 murine embryonic fibroblasts were seeded 1 day after seeding, following infection with *Plasmodium vivax* sporozoites.

P. vivax Infection of MPCCs

30,000 to 60,000 sporozoites were overlaid onto MPCC cultures (5,000 for 384 MPCCs), seeded the day before, in hepatocyte medium and kept at 37°C and 5% CO2 for 3 hours for infection to occur. Post-infection, wells were washed twice and fresh media containing fibroblasts was added. Cultures were fixed on days 5, 8, 9, 10, 11, 18 and 21 for in paraformaldehyde (PFA) or ice-cold methanol for analysis by immunofluorescence.

Human Reticulocyte Overlay

Adult human blood from the Thai Red Cross was passed through Pall filters (Pall Corporation) to remove leukocytes. Remaining red blood cells were washed with RPMI1640 and collected via centrifugation (100 g, 10 min). Packed cells were resuspended in OptiPrep (Axis Shield) and KCl buffer and centrifuged at 3,000 g for 30 minutes. Reticulocytes were collected from the interface and washed with RPMI1640 then resuspended to 50% hematocrit. Reticulocyte enrichment was calculated by methylene blue staining. $33x10^6$ red blood cells (of which 33% were reticulocytes) were overlaid per well of the 96-well MPCC, diluted in hepatocyte medium. Fresh media containing red blood cells was added daily.

Drug Treatment of *P. vivax* EEFs in MPCCs

Infected MPCCs were incubated with media containing the drug being tested (primaquine diphosphate (Sigma) ranging from 0.1–10 μM, atovaquone (Sigma) ranging from 0.1 to 270nM; MMV390048, MMV67494 KDU691, LMV599, KAF156, DDD107498 (Medicines for Malaria Venture) ranging from 0.03 μM to 10 μM. For prophylactic treatment, fresh drug-containing medium was added daily until day 5 with drug-free media changes until fixation on day 8. For radical cure treatment, fresh drug-containing medium was added daily from day 5 until day 8 when cultures were fixed. IC_{50} curves were generated by plotting the number of parasites left in culture, compared to control, under varying doses of drug.

Immunofluorescence Staining

MPCCs were fixed with either ice-cold methanol for 10 minutes at 4°C or 4% paraformaldehyde (PFA) for 20 minutes at room temperature. PFA-fixed samples were permeabilized with 0.1% TritonX for 10 minutes at room temperature. Wells were washed twice with PBS, blocked with 2% bovine serum albumin (BSA) in phosphate-buffered saline (PBS), and incubated with primary antibodies for 1 hour at room temperature. Samples were washed with PBS then incubated with Alexa 546-conjugated secondary goat-anti-mouse (Invitrogen) and Alexa 647-conjugated goat anti-rabbit (Invitrogen) for 1 hour at room temperature. Samples were washed with PBS, counterstained with the DNA dye Hoechst 33258 (Invitrogen; 1:5,000), and kept in Aquamount (Lerner Laboratories). Images were captured on a Nikon Eclipse Ti fluorescence microscope or a Nikon 1AR Ultra-Fast confocal microscope. Areas of the developing liver-stage parasites were measured using ImageJ and used to calculate the corresponding diameter. Liver-stage *P. vivax* parasites were detected using rabbit polyclonal antibodies against UIS4, BIP, MIF, HSP60, HSP70, MSP1 and mouse monoclonal antibodies against UIS4 and ACP. The nuclei of the parasites were visualized using a rabbit polyclonal anti-acetyl-Histone H3 (Lys9) antibody (Millipore).

Hybrid Capture, RNA-seq Extraction and Analysis

SureSelectXT RNA Direct capture probes were designed for the *P. vivax* P01 genome using eArray with the assistance of Agilent Technologies. Preliminary RNA-seq experiments revealed significant transcription outside the annotated gene loci *in P. vivax* (data not shown). To accommodate novel transcripts, probes were designed to tile the *P. vivax* genome such that they included all known genes and intergenic regions while specifically excluding rRNA transcripts, known pseudogenes and regions with homology to human or mouse. Design is available as ELID: S3090564

Total RNA was extracted using TRIzol (Thermo Fisher) and purified using RNeasy Mini Kit (Qiagen) according to manufacturer's instructions. Samples were DNase treated. RNA was quality controlled using an AATI Fragment Analyzer and 100ng was prepared following the SureSelectXT RNA Direct protocol version A0. Illumina libraries were quantitated using the Fragment Analyzer and by qPCR and sequenced as a single end 40nt read using a HiSeq2000.

Quantitative RT-PCR

Total RNA was extracted with TRIzol (Thermo Fisher), DNAse treated and purified using the RNeasy MinElute Cleanup Kit (Qiagen). cDNA synthesis was performed using SuperScript II (Thermo Fisher) and RT-PCR was carried out using PowerUp SYBR Green Master Mix (Applied Biosystems) in a Roche Light Cycler 480 Real-Time PCR Detection System according to the manufacturer's instructions. The primers used are listed in Table S2. Relative gene expression was calculated with the $\Delta\Delta Ct$ method, using PVP01_1213400 as housekeeping gene.

QUANTIFICATION AND STATISTICAL ANALYSIS

Sample Sizes and Statistical Analysis

n represents the number wells from each plate as described in the figure legends. Data were analyzed using Prism 7.0 (GraphPad Software, San Diego, CA) and results represent means ± SEM. Methods used for computing statistical significance is indicated in figure legends. Statistically significant differences were defined as * when p values were < 0.05, ** $p < 0.01$, *** $p < 0.001$, and **** $p < 0.0001$. To avoid plate position effects, setups of all conditions were randomly assigned in each experiment. Drugs tested in Figures 3B–3D were blinded and scored by independent researchers.

RNA-seq Data

Illumina Offline BaseCaller1.9.3 software was used for basecalling. Reads were aligned against Plasmodium vivax PvP01 from PlasmoDB v. 34 (Sept 2017) using STAR v. 2.5.3a (Dobin et al., 2013) with flags -runThreadN 8 –runMode alignReads –outFilterType BySJout –outFilterMultimapNmax 20 –alignSJoverhangMin 8 –alignSJDBoverhangMin 1 –outFilterMismatchNmax 999 –alignIntronMin 10 –alignIntronMax 1000000 –alignMatesGapMax 1000000 –outSAMtype BAM SortedByCoordinate –quantMode TranscriptomeSAM with –genomeDir pointing to a 75nt-junction PvivaxP01 STAR suffix array.

Gene expression was quantitated using RSEM v. 1.3.0 (Li and Dewey, 2011) with the following flags for all libraries: rsem-calculate-expression –calc-pme –alignments -p 8 –forward-prob 0 against an annotation matching the STAR SA reference. Posterior mean estimates (pme) of counts were retrieved, and transcripts corresponding to rRNAs and tRNAs were removed.Resulting read counts were summarized by genes, then converted into RPKMs using RSEM effective gene length estimates, and finally to TPMs.

For principal components analysis (PCA), log-transformed, quantile-normalized TPM data were processed using a singular-value decomposition approach (SVD) as implemented in the prcomp function in the R statistical environment (v. 3.4.0). Gene loadings for each gene for component 1 were extracted and ranked.

Differential-expression analysis was performed using DESeq2 on the rRNA-substracted raw counts (Anders and Huber, 2010; Love et al., 2014) Briefly, sequencing library size factors were estimated for each library, and differences in gene expression between conditions (expressed as log2-transformed fold-changes in expression levels) were estimated under a general linear model (GLM) framework fitted on the read counts. In this model, read counts of each gene in each sample were modeled under a negative binomial distribution, based on the fitted mean of the counts and aforementioned dispersion parameters. Differential expression significance was assessed using a Wald test on the fitted count data (all these steps were performed using the DESeq() function in DESeq2). Genes with at least a two-fold change between "Mixed" and "Hypnozoite" sample groups (with adjusted p values <0.01 using Benjamini-Hochberg procedure (Benjamini and Hochberg, 1995) were selected for downstream analysis.

For heat map generation, median log-transformed TPM values were calculated for each gene and the log2-fold-changes over the median was calculated for each sample. The resulting matrix was subjected to hierarchical clustering using 1-Pearson correlation as a distance metrics and a [complete-single-sample average] linkage function.

DATA AND SOFTWARE AVAILABILITY

Raw Data

Raw RNA-seq data have been deposited into the Gene Expression Omnibus (GEO) under the accession number GSE108016.